

TECHNICAL RESEARCH REPORT

Control of Hysteresis in Smart Actuators, Part II: A Robust Control Framework

by Xiaobo Tan, John S. Baras

CDCSS TR 2002-9
(ISR TR 2002-55)



The Center for Dynamics and Control of Smart Structures (CDCSS) is a joint Harvard University, Boston University, University of Maryland center, supported by the Army Research Office under the ODDR&E MURI97 Program Grant No. DAAG55-97-1-0114 (through Harvard University). This document is a technical report in the CDCSS series originating at the University of Maryland.

Web site <http://www.isr.umd.edu/CDCSS/cdcss.html>

Report Documentation Page				Form Approved OMB No. 0704-0188	
Public reporting burden for the collection of information is estimated to average 1 hour per response, including the time for reviewing instructions, searching existing data sources, gathering and maintaining the data needed, and completing and reviewing the collection of information. Send comments regarding this burden estimate or any other aspect of this collection of information, including suggestions for reducing this burden, to Washington Headquarters Services, Directorate for Information Operations and Reports, 1215 Jefferson Davis Highway, Suite 1204, Arlington VA 22202-4302. Respondents should be aware that notwithstanding any other provision of law, no person shall be subject to a penalty for failing to comply with a collection of information if it does not display a currently valid OMB control number.					
1. REPORT DATE 2002		2. REPORT TYPE		3. DATES COVERED -	
4. TITLE AND SUBTITLE Control of Hysteresis in Smart Actuators, Part II: A Robust Control Framework				5a. CONTRACT NUMBER	
				5b. GRANT NUMBER	
				5c. PROGRAM ELEMENT NUMBER	
6. AUTHOR(S)				5d. PROJECT NUMBER	
				5e. TASK NUMBER	
				5f. WORK UNIT NUMBER	
7. PERFORMING ORGANIZATION NAME(S) AND ADDRESS(ES) Army Research Office,PO Box 12211,Research Triangle Park,NC,27709				8. PERFORMING ORGANIZATION REPORT NUMBER	
9. SPONSORING/MONITORING AGENCY NAME(S) AND ADDRESS(ES)				10. SPONSOR/MONITOR'S ACRONYM(S)	
				11. SPONSOR/MONITOR'S REPORT NUMBER(S)	
12. DISTRIBUTION/AVAILABILITY STATEMENT Approved for public release; distribution unlimited					
13. SUPPLEMENTARY NOTES The original document contains color images.					
14. ABSTRACT see report					
15. SUBJECT TERMS					
16. SECURITY CLASSIFICATION OF:			17. LIMITATION OF ABSTRACT	18. NUMBER OF PAGES 28	19a. NAME OF RESPONSIBLE PERSON
a. REPORT unclassified	b. ABSTRACT unclassified	c. THIS PAGE unclassified			

Control of Hysteresis in Smart Actuators, Part II: A Robust Control Framework

Xiaobo Tan* and John S. Baras

Institute for Systems Research and

Department of Electrical and Computer Engineering

University of Maryland, College Park, MD 20742 USA

{xbtan, baras}@isr.umd.edu

Abstract

Hysteresis in smart actuators presents a challenge in control of these actuators. A fundamental idea to cope with hysteresis is inverse compensation. But due to the open loop nature of inverse compensation, its performance is susceptible to model uncertainties and to errors introduced by inverse schemes. In this paper we develop a robust control framework for smart actuators by combining inverse control with the l_1 robust control theory. We show that, for both the rate-independent hysteresis model and the rate-dependent one, the inversion error can be bounded in magnitude and the bound is quantifiable in terms of parameter uncertainties and the inversion scheme. Hence we can model the inversion error as an exogenous disturbance and attenuate its impact by robust control techniques. Through the example of controlling a magnetostrictive actuator, we present a systematic controller design method which guarantees robust stability and robust trajectory tracking while taking actuator saturation into account. Simulation and experimental results are provided.

Keywords: Hysteresis; Smart Actuators; Robust control; Inverse compensation; Actuator saturation

*Corresponding author.

1 Introduction

Smart materials, such as magnetostrictives, piezoelectrics, shape memory alloys (SMAs), and magnetorheological (MR) fluids, all display coupling phenomena between applied electromagnetic/thermal fields and their mechanical/rheological properties. Smart actuators and sensors made of these materials have been receiving tremendous interest due to their broad applications in areas of aerospace, manufacturing, defense, and civil infrastructure systems, to name a few. The hysteretic behavior widely existing in smart materials, however, makes the effective use of these actuators and sensors quite challenging.

Models for smart actuators that capture both hysteresis and dynamic behaviors have a cascaded structure as shown in Figure 1(a) [1], where W is a hysteretic operator (with possibly some other nonlinearities) and $\hat{G}_a(\lambda)$ is a linear system. In this paper we consider the discrete-time setting in the interest of digital control, and $\hat{G}(\lambda)$ denotes the λ -transform of a linear time-invariant (LTI) system G . We recall that the λ -transform $\hat{G}(\lambda)$ is just the usual z -transform of G with $\lambda = z^{-1}$ [2].

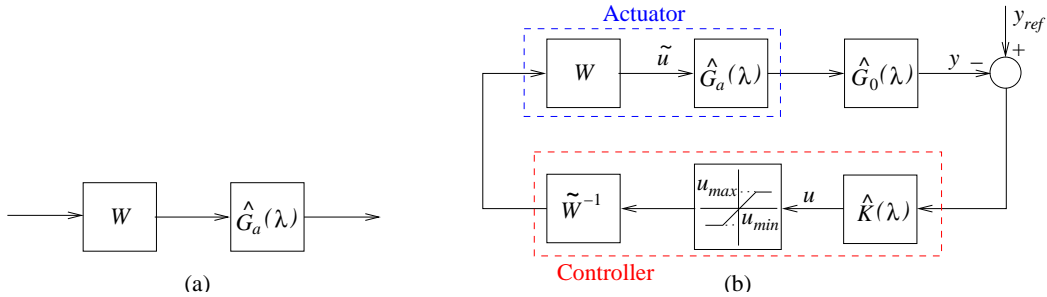


Figure 1: (a) The model structure for smart actuators; (b) The closed-loop system incorporating inverse compensation.

In Figure 1(b), $\hat{G}_0(\lambda)$ denotes the plant to be controlled by the actuator. A basic approach to cope with the hysteresis is to construct an (approximate) right inverse operator \tilde{W}^{-1} for W , then $\tilde{u} \approx u$ and the controller design problem is reduced to designing a linear controller $\hat{K}(\lambda)$ for the composite linear system $\hat{G}_0(\lambda) \circ \hat{G}_a(\lambda)$. The idea of inverse compensation can be found in, e.g., [3, 4, 5, 6, 7].

The most popular hysteresis model used in control of smart actuators has been the Preisach operator [3, 8, 9, 7]. The Preisach operator provides a means of developing phenomenological models that are capable of producing behaviors similar to those of physical systems. For a detailed treatment of the Preisach operator, we refer to [10, 11, 12]. In Part I of this two-part paper [13], we studied

modeling and inverse control of smart actuators based on a magnetostrictive actuator. In particular, we modeled the rate¹-independent hysteresis with essentially a Preisach operator alone, and the rate-dependent hysteresis with a Preisach operator coupled to an ordinary differential equation (ODE). We also presented identification methods and efficient real-time inversion schemes for these models in [13].

Due to the open loop nature of inverse compensation, its performance is susceptible to model uncertainties and to errors introduced by inversion schemes. To combat this problem, adaptive inverse control schemes have been proposed for a class of hysteresis nonlinearities with parameterizable inverses [4, 14, 15]. For the Preisach operator-based hysteresis models, however, their inverses are not parameterizable in general. In this paper we develop a robust control framework for smart actuators by combining inverse control with the l_1 control techniques. We show that, for both the rate-independent hysteresis model and the rate-dependent one, the inversion error can be bounded in magnitude and the bound is quantifiable in terms of parameter uncertainties and the inversion scheme. Hence we can model the inversion error as an exogenous disturbance and attenuate its impact by robust control techniques.

The design requirements for the controller $\hat{K}(\lambda)$ can be roughly stated as: in the presence of the inversion error and the uncertainties in \hat{G}_a and \hat{G}_0 , for all desired trajectories in a certain class,

1. The closed-loop system is stable;
2. The tracking error is minimized;
3. The output of \hat{K} does not exceed the saturation limits.

We take the saturation constraint (a common nonlinearity in actuators) into account in the design of \hat{K} to ensure that the overall system operates in the linear region and thus predictions based on the linear design are credible. The controller design method will be illustrated through the example of robust trajectory tracking of a magnetostrictive actuator.

As remarked in [13], choosing control of the magnetostrictive actuator as an example allows us to cover both the rate-independent hysteresis case and the rate-dependent hysteresis case. The approach presented here applies directly to control of a wide class of smart actuators.

¹Throughout the paper, the word “rate” is referred to how fast the input is being varied. For a periodic input, the rate is directly related to its frequency.

The remainder of the paper is organized as follows. In Section 2 we introduce the Preisach operator and review an identification scheme for the Preisach operator. In Section 3 we describe the model for a magnetostrictive actuator. We discuss quantification of bounds on inversion errors in Section 4. We then formulate and solve the robust control problem in Section 5. Simulation and experimental results are provided in Section 6. Finally we conclude in Section 7.

A preliminary version of some results in this paper was submitted for presentation at 2003 American Control Conference [16].

2 The Preisach Operator

For a pair of thresholds (β, α) with $\beta \leq \alpha$, consider a simple hysteretic element $\hat{\gamma}_{\beta, \alpha}[\cdot, \cdot]$, as illustrated in Figure 2. For $u \in C([0, T])$ and an initial configuration $\zeta \in \{-1, 1\}$, the function

$$v = \hat{\gamma}_{\beta, \alpha}[u, \zeta] : [0, T] \rightarrow \{-1, 1\}$$

is defined as follows [11]:

$$v(0) \triangleq \begin{cases} -1 & \text{if } u(0) \leq \beta \\ \zeta & \text{if } \beta < u(0) < \alpha \\ 1 & \text{if } u(0) \geq \alpha \end{cases} ,$$

and for $t \in (0, T]$, setting $X_t \triangleq \{\tau \in (0, t] : u(\tau) = \beta \text{ or } \alpha\}$,

$$v(t) \triangleq \begin{cases} v(0) & \text{if } X_t = \emptyset \\ -1 & \text{if } X_t \neq \emptyset \text{ and } u(\max X_t) = \beta \\ 1 & \text{if } X_t \neq \emptyset \text{ and } u(\max X_t) = \alpha \end{cases} .$$

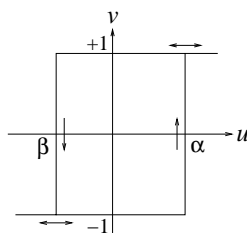


Figure 2: The elementary Preisach hysteron.

This operator is sometimes referred to as an *elementary Preisach hysteron* (we will call it a *hysteron* in this paper), since it is a building block for the Preisach operator.

The Preisach operator is a weighted superposition of all possible hysterons. Define

$$\mathcal{P}_0 \triangleq \{(\beta, \alpha) \in \mathbb{R}^2 : \beta \leq \alpha\}.$$

\mathcal{P}_0 is called the *Preisach plane*, and each $(\beta, \alpha) \in \mathcal{P}_0$ is identified with the hysteron $\hat{\gamma}_{\beta, \alpha}$. For $u \in C([0, T])$ and a Borel measurable initial configuration ζ_0 of all hysterons, $\zeta_0 : \mathcal{P}_0 \rightarrow \{-1, 1\}$, the output of the Preisach operator Γ is defined as [11]:

$$z(t) = \Gamma[u, \zeta_0](t) = \int_{\mathcal{P}_0} \hat{\gamma}_{\beta, \alpha}[u, \zeta_0(\beta, \alpha)](t) d\nu(\beta, \alpha), \quad (1)$$

where ν is a finite, signed Borel measure on \mathcal{P}_0 , called the *Preisach measure*.

We call the Preisach measure ν *nonsingular* if $|\nu|$ is absolutely continuous with respect to the two-dimensional Lebesgue measure. By the Radon-Nikodym theorem [17], if ν is nonsingular, there exists a Borel measurable function μ , such that

$$\Gamma[u, \zeta_0](t) = \int \int_{\mathcal{P}_0} \mu(\beta, \alpha) \hat{\gamma}_{\beta, \alpha}[u, \zeta_0(\beta, \alpha)](t) d\beta d\alpha. \quad (2)$$

The weighting function μ is often referred to as the *Preisach function* [10] or the *density function* [12]. We consider exclusively the case $\mu \geq 0$ in this paper.

To simplify the discussion, throughout the paper we assume that μ has a compact support, i.e., $\mu(\beta, \alpha) = 0$ if $\beta < \beta_0$ or $\alpha > \alpha_0$ for some β_0, α_0 , and without loss of generality, we let $\alpha_0 = -\beta_0 =: r_0 > 0$. Then it suffices to consider the finite triangular area $\mathcal{P} \triangleq \{(\beta, \alpha) \in \mathbb{R}^2 | \alpha \geq \beta, \beta \geq -r_0, \alpha \leq r_0\}$.

At time t , \mathcal{P} can be divided into two regions: $\mathcal{P}_{\pm}(t) \triangleq \{(\beta, \alpha) \in \mathcal{P} | \text{output of } \hat{\gamma}_{\beta, \alpha} \text{ at } t \text{ is } \pm 1\}$. In most cases of interest, each of \mathcal{P}_- and \mathcal{P}_+ is a connected set [10], and the output of Γ is determined by the boundary between \mathcal{P}_- and \mathcal{P}_+ if the Preisach measure is nonsingular. The boundary is also called the *memory curve*. The memory curve typically has a staircase structure and its intersection with the line $\alpha = \beta$ gives the current input value. For a precise characterization of the *set Ψ of memory curves*, we refer to [18]. The memory curve ψ_0 at $t = 0$ is called the *initial memory curve* and it represents the initial condition of the Preisach operator.

If the Preisach measure is nonsingular, we can identify a configuration of hysterons ζ_{ψ} with a memory curve ψ in the following way: $\zeta_{\psi}(\beta, \alpha) = 1$ (-1 , resp.) if (β, α) is below (above, resp.) the

graph of ψ . Note that it does not matter whether ζ_ψ takes 1 or -1 on the graph of ψ . In the sequel we will put the initial memory curve ψ_0 as the second argument of Γ , where $\Gamma[\cdot, \psi_0] \triangleq \Gamma[\cdot, \zeta_{\psi_0}]$.

A constrained least squares scheme was proposed to identify the Preisach measure ν in [7]. In the scheme, the input is discretized into $L + 1$ levels (called *discretization of level L*) for some $L > 0$ and that leads to a discretized Preisach operator (Figure 3), i.e., a weighted sum of finitely many hysterons. What is identified in [7], is a collection of weighting masses sitting at centers of cells in the discretization grid (see the dark dots in Figure 3). We can then obtain a nonsingular approximation ν_p to the true Preisach measure ν by assuming that each identified mass is distributed uniformly over the corresponding cell. Note that the density μ_p corresponding to ν_p is piecewise uniform.

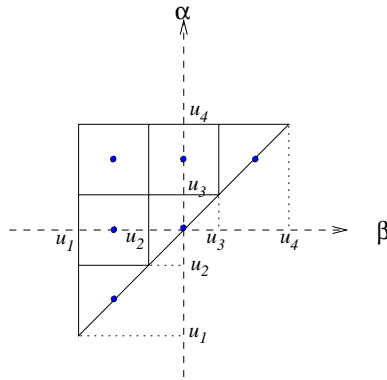


Figure 3: Discretization of the Preisach plane ($L = 3$).

3 The Model for Thin Magnetostrictive Actuators

Magnetostriction is the phenomenon of strong coupling between magnetic properties and mechanical properties of some ferromagnetic materials (e.g., Terfenol-D). Figure 4 shows a sectional view of a thin Terfenol-D actuator. By varying the current in the coil, we vary the magnetic field in the Terfenol-D rod and thus control the displacement of the rod head. Figure 5 displays the hysteresis observed in the magnetostrictive actuator.

When the frequency of the input current is low (typically below 5 Hz), the magnetostrictive hysteresis is rate-independent – roughly speaking, the shape of the hysteresis loop is independent of

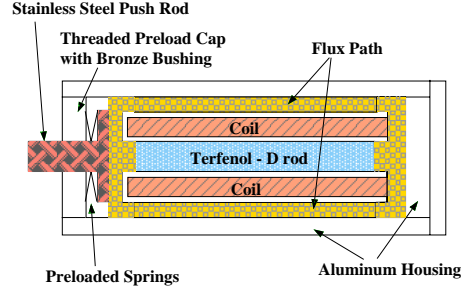


Figure 4: Sectional view of a Terfenol-D actuator [19](Original source: Etrema Products, Inc.).

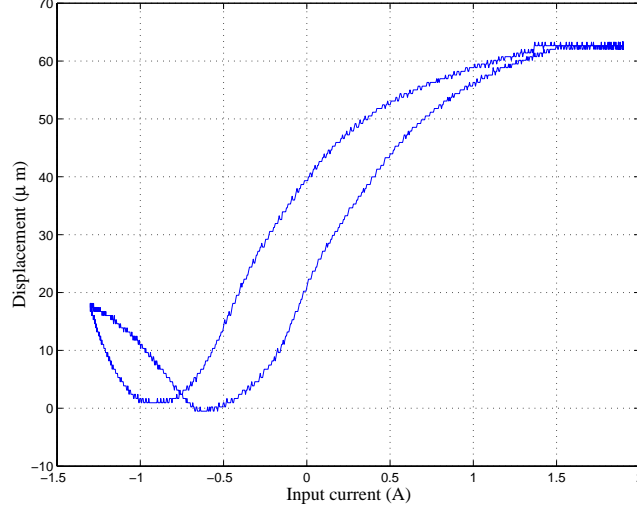


Figure 5: Hysteresis in a magnetostrictive actuator.

the input frequency, and it can be modeled by *essentially* a Preisach operator ² [7]:

$$\begin{cases} H(t) = c_0 I(t) \\ M(t) = \Gamma[H(\cdot), \psi_0](t) \\ y(t) = c_M M^2(t) \end{cases} \quad , \quad (3)$$

where I is the input current, y is the displacement of the actuator head, M and H are the bulk magnetization and the magnetic field (assumed uniform) along the rod direction, respectively, Γ is the Preisach operator, and c_0 and c_M are positive constants.

When the input frequency gets high, the magnetostrictive hysteresis is rate-dependent. Venkataraman and Krishnaprasad proposed a bulk magnetostrictive hysteresis model for the thin rod actuator based on energy balancing principles [20, 19]. The model has a cascaded structure as shown in Figure 6. Note the resemblance of Figure 6 with Figure 1(a). \bar{W} takes care of the $M - H$ hysteresis and

²To ease discussion, we have absorbed the (constant) bias field H_{bias} [13] into $I(t)$.

the eddy current losses, and the magnetoelastic dynamics of the rod is lumped into a second order linear system $G(s)$. $G(s)$ has a state space representation [20, 19](after some manipulations):

$$\ddot{y}(t) + 2\xi\omega_0\dot{y}(t) + \omega_0^2 y(t) = \omega_0^2 c_M M^2(t), \quad (4)$$

where ω_0 and ξ are positive constants.

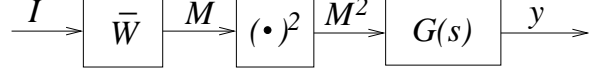


Figure 6: Model structure of a magnetostrictive actuator.

By replacing the switching ODE model in [20, 19] with a Preisach operator Γ for the $M - H$ hysteresis, we have proposed a new dynamic model [13, 18] for the \bar{W} block:

$$\begin{cases} \dot{H}(t) + \dot{M}(t) = c_1(I(t) - \frac{H(t)}{c_0}) \\ M(t) = \Gamma[H(\cdot), \psi_0](t) \end{cases}, \quad (5)$$

where c_1 is a positive constant. We note that the Preisach operator is coupled to an ODE in an unusual way in (5).

We also note that setting derivatives in (4) and (5) to zero, the dynamic model degenerates to the rate-independent hysteresis model (3). More details on magnetostrictive actuators and the modeling can be found in [13].

4 Quantification of the Inversion Error

Recall Figure 1(b). In general \tilde{W}^{-1} is not an exact (right) inverse of W , and two factors may contribute to the inversion error e_u : parameter uncertainties in W and non-existence of exact inverse schemes.

There are two possible ways to model e_u . One is to model it as the output of some uncertainty block Δ (Figure 7(a)), and the other is to simply model it as an exogenous disturbance v (Figure 7(b)). For the Preisach operator-based models, e_u is independent of u and it is possible that $e_u \neq 0$ for $u = 0$. Therefore there exists no stable Δ such that $e_u = \Delta u$, and we will treat $e_u = v$ as an external noise.

We need specify the signal spaces for quantification of the inversion error. The inversion error for the Preisach operator is bounded in magnitude instead of in energy. Hence a natural choice for the

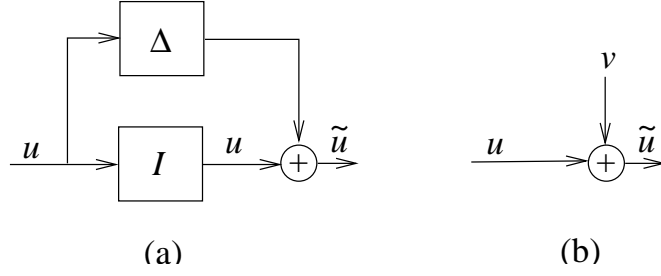


Figure 7: Two ways to represent the inversion error.

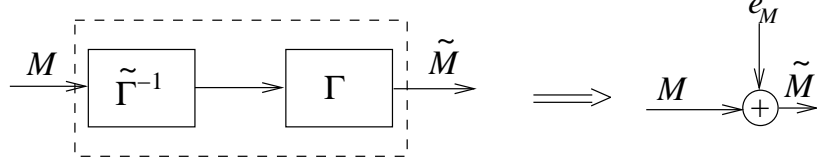


Figure 8: The error in inversion of the Preisach operator.

signal spaces is l_∞ and not l_2 . Also it is more appropriate to use l_∞ for the desired trajectory and the tracking error. Another advantage of using l_∞ for signals is that the actuator saturation constraint can be easily handled in the corresponding l_1 robust control theory, while it's very hard to be formulated in \mathcal{H}_∞ control theory.

We now quantify the error bounds in inversion of the Preisach operator and the dynamic model (5). Here we are concerned with $e_M[\cdot] = \tilde{M}[\cdot] - M[\cdot]$, where $\tilde{M}[\cdot]$ and $M[\cdot]$ denote the trajectories of achieved output and desired output of the Preisach operator, respectively. The bound on e_u when the square nonlinearity in Figure 6 is included can be easily derived from the bound on e_M .

We will not review the inversion algorithms here, since they have been given in [13]. Interested readers are referred to [13] or [18] for details.

4.1 Error in inversion of the Preisach operator with a nonsingular measure

Consider Figure 8, where Γ is a Preisach operator with nonsingular Preisach measure ν .

Given a sequence $\{M[k]\} \in l_\infty$ and the initial memory curve $\psi_0 \in \Psi$ (the set of memory curves), the inversion problem for the Preisach operator is to find the input sequence $\{H[k]\} \in l_\infty$, such that

the output sequence $\{\tilde{M}[k]\}$ matches $\{M[k]\}$, i.e.,

$$M[k] = \Gamma[H[\cdot], \psi_0][k].$$

Remark 4.1 *Note that we now have a sequence instead of a continuous time function as the first argument of Γ . To avoid confusion, we tacitly understand that the input is monotonically changed from $H[k]$ to $H[k+1]$. Throughout the paper we may use a sequence or a continuous time function as the first argument of Γ depending on the context.*

As discussed in [13], for a Preisach operator with a nonnegative, nonsingular Preisach measure, the inversion problem can be solved with arbitrary accuracy if the Preisach measure is known exactly. In this case, it suffices to consider the inversion problem of length 1: given $\psi_0 \in \Psi$ and $\bar{M} \in [-M_s, M_s]$, where M_s is the saturation output of the Preisach operator, find \bar{H} such that

$$\bar{M} = \Gamma[\bar{H}, \psi_0]. \quad (6)$$

4.1.1 Error due to the inversion scheme

If the Preisach measure ν is known exactly but otherwise has a general distribution, an iterative algorithm is available to solve (6) with arbitrary accuracy [13]. Let the stopping criterion be $|M^{(n)} - \bar{M}| \leq \epsilon$, where $M^{(n)}$ denotes the output value of Γ achieved at the n -th iteration. Then it's straightforward that

$$\|e_M\|_\infty \leq \epsilon \text{ for any } M[\cdot] \in l_\infty.$$

4.1.2 Error due to the parameter uncertainty

If the Preisach measure ν is unknown, we can obtain a nonsingular approximation ν_p with a piecewise uniform density μ_p as discussed in Section 2. The Preisach operator with measure ν_p can be inverted exactly (in a finite number of steps) [13]. Hence the inversion error e_M is now solely due to the measure uncertainty $|\nu - \nu_p|$. It turns out that we can quantify the error bound in terms of the relative identification error and the discretization level L of the Preisach plane:

Proposition 4.1 *Let the true Preisach measure ν be nonnegative and nonsingular with density μ . Let μ be bounded by some constant $\bar{\mu} > 0$. Given a discretization of level L , denote the integral of μ*

over a cell i as ν_i^0 , $1 \leq i \leq N_c$, where N_c is the total number of cells. Denote by ν_i the identified mass for cell i . Assume the relative error in identification is δ_I , i.e., $\frac{|\nu_i - \nu_i^0|}{\nu_i^0} \leq \delta_I$, $1 \leq i \leq N_c$. Then

$$\|e_M\|_\infty \leq \delta_I M_s + \frac{8\bar{\mu}r_0^2}{L},$$

where M_s is the saturation output of the Preisach operator with measure ν , and r_0 is as defined in Section 2.

Proof. Define μ_p as discussed earlier. We obtain another Preisach measure with a piecewise constant density μ_p^0 by distributing ν_i^0 uniformly over the cell i , $1 \leq i \leq N_c$. To distinguish the Preisach operators, we will put the corresponding density as the subscript of Γ , e.g., Γ_μ denotes the Preisach operator with Preisach density μ .

Given $M[\cdot] \in l_\infty$ and ψ_0 , we denote the output of $\tilde{\Gamma}^{-1}$ in Figure 8 as H , where $\tilde{\Gamma}^{-1}$ is the inverse of Γ_{μ_p} . Then, $\forall k \geq 0$,

$$\begin{aligned} |e_M[k]| &= |\Gamma_\mu[H, \psi_0][k] - \Gamma_{\mu_p}[H, \psi_0][k]| \\ &\leq |\Gamma_\mu[H, \psi_0][k] - \Gamma_{\mu_p^0}[H, \psi_0][k]| + |\Gamma_{\mu_p^0}[H, \psi_0][k] - \Gamma_{\mu_p}[H, \psi_0][k]|. \end{aligned} \quad (7)$$

All three Preisach operators involved in (7) share the same memory curve $\psi[k]$, $\forall k \geq 0$. It's obvious that the second term of (7) is bounded by $\delta_I M_s$. To bound the first term, we note that for any $k \geq 0$, the memory curve $\psi[k]$ spans $L-1$ square cells and one triangular cell (Figure 9). Any cell not touched by $\psi[k]$ will contribute the same amount to $\Gamma_\mu[H, \psi_0][k]$ and $\Gamma_{\mu_p^0}[H, \psi_0][k]$. Hence the first term of (7) is bounded by twice the integral of μ over cells spanned by $\psi[k]$, which is further bounded by

$$\frac{2\bar{\mu}(2r_0)^2(L - \frac{1}{2})}{L^2} < \frac{8\bar{\mu}r_0^2}{L}.$$

This completes the proof. \square

Remark 4.2 From Proposition 4.1, the bound on the inversion error consists of two parts: the first part is proportional to the relative identification error, and the second part is inversely proportional to the level L of discretization.

Remark 4.3 The assumption that ψ_0 is known is not very restrictive since in many cases we have the choice to initialize the system. On the other hand, if ψ_0 is not known exactly, we can easily include a term in $\|e_M\|_\infty$ which takes care of the uncertainty in ψ_0 .

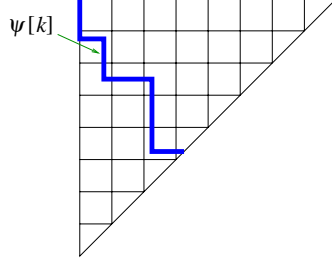


Figure 9: Illustration of the proof of Proposition 4.1 ($L = 8$).

4.2 Error in inversion of the dynamic hysteresis model

Given the initial memory curve ψ_0 and a trajectory of $M(\cdot)$, inversion of (5) is to find $I(\cdot)$, so that the output of the block \bar{W} in Figure 6 is $M(\cdot)$. The following (formal) inversion scheme was proposed in [13]:

$$I(t) = \frac{1}{c_1}(\dot{H}(t) + \dot{M}(t)) + \frac{H(t)}{c_0}, \quad (8)$$

where $H(t) = \Gamma^{-1}[M(\cdot), \psi_0](t)$. But if there is uncertainty in the model parameters, it is very hard to derive a bound for the inversion error. We now present another inversion algorithm. This algorithm leads to an inversion error even if the exact parameters are known, but it will allow us to quantify the inversion error when model uncertainties are present.

Eq. (5) can be rewritten as:

$$\begin{cases} \dot{H}(t) = \frac{c_1}{1+g(t)}(I(t) - \frac{H(t)}{c_0}) \\ M(t) = \Gamma[H(\cdot), \psi_0](t) \end{cases}, \quad (9)$$

where $g(t)$ carries the interpretation of “ $\frac{dM}{dH}$ ” at time t , and it depends on both the state ψ_t (the memory curve at t) and the sign of \dot{H} [18]. When the Preisach measure is nonnegative and nonsingular with a piecewise continuous density, we have $0 \leq g(t) \leq C_g$, for some constant $C_g > 0$ [18]. We can view (9) as perturbed from the following decoupled system:

$$\begin{cases} \dot{H}(t) = \frac{c_1}{1+\bar{g}}(I(t) - \frac{H(t)}{c_0}) \\ M(t) = \Gamma[H(\cdot), \psi_0](t) \end{cases}, \quad (10)$$

where $\bar{g} \in [0, C_g]$ is some constant (at our disposal). Based on (10), an *approximate* inversion scheme for (9) is given formally by

$$\begin{cases} H(t) = \Gamma^{-1}[M(\cdot), \psi_0](t) \\ I(t) = \frac{1+\bar{g}}{c_1}\dot{H}(t) + \frac{H(t)}{c_0} \end{cases}. \quad (11)$$

We have two ways to implement the second equation in (11) in the discrete time, which correspond to the explicit Euler scheme and the implicit Euler scheme in discretizing the first equation in (10), respectively: for $k \geq 0$,

$$I[k] = \frac{1 + \bar{g}}{c_1 h} (H[k] - H[k-1]) + \frac{H[k-1]}{c_0}, \quad (12)$$

$$I[k] = \frac{1 + \bar{g}}{c_1 h} (H[k] - H[k-1]) + \frac{H[k]}{c_0}, \quad (13)$$

where h is the time step size, $H[-1] = H[0]$.

Remark 4.4 *Direct discretization of the first equation in (10) by the explicit Euler scheme (a similar remark applies to the implicit Euler scheme) gives:*

$$I[k] = \frac{1 + \bar{g}}{c_1 h} (H[k+1] - H[k]) + \frac{H[k]}{c_0},$$

but this is not a causal system and thus not realizable. An intrinsic delay is introduced in the inversion due to the dynamics in the rate-dependent hysteresis model.

We now want to study the errors caused exclusively by the inversion algorithms, i.e., we assume that we have exact values of parameters. For the algorithm (12), the discrete-time version of the first equation in (9) is obtained by the explicit Euler scheme:

$$\frac{\tilde{H}[k+1] - \tilde{H}[k]}{h} = \frac{c_1}{1 + g[k]} (I[k] - \frac{\tilde{H}[k]}{c_0}), \quad (14)$$

where $g[k] \triangleq g(kh)$. Similarly, if the inversion algorithm (13) is used, we will use the corresponding discrete-time model obtained by the implicit Euler scheme. Figure 10(a) shows the problem setup for the explicit Euler case.

For the purpose of deriving the bound on the inversion error, we will not need the exact values of $g[k]$. Due to the delay caused by the inversion, the error e_M is now defined as (Figure 10(d)):

$$e_M[k] \triangleq \tilde{M}[k] - M[k-1].$$

Proposition 4.2 *Let the Preisach measure be nonnegative and nonsingular with a piecewise continuous density μ . Let the Preisach operator Γ be Lipschitz continuous with Lipschitz constant L_μ . Consider the inversion algorithm obtained from the explicit Euler method (Figure 10(a)). Let $H[-1] = H[0] = \tilde{H}[0]$. Pick $\bar{g} \in [0, C_g]$. Then for any $M[\cdot] \in l_\infty$, for any $\psi_0 \in \Psi$,*

$$\|e_M\|_\infty \leq 2L_\mu \bar{\gamma}_e r_0, \quad (15)$$

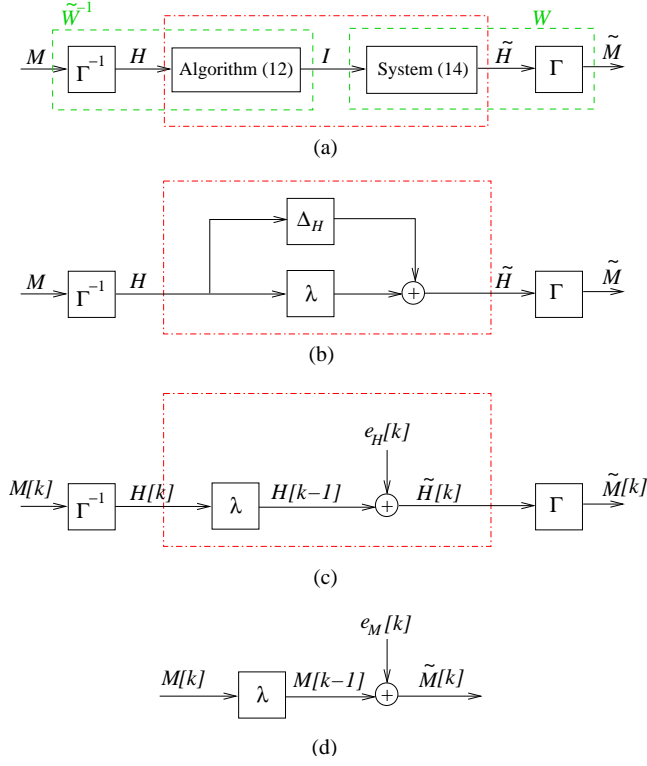


Figure 10: The error in inversion of the rate-dependent hysteresis model.

where

$$\bar{\gamma}_e = \frac{\max\{\bar{g}, \frac{C_g - \bar{g}}{1 + C_g}\}}{1 - \max\{\frac{hc_1}{c_0} - 1, 1 - \frac{hc_1}{c_0(1 + C_g)}\}}.$$

The optimal \bar{g} to minimize $\bar{\gamma}_e$ is $\frac{C_g}{C_g + 2}$.

Proof. We first derive a bound for e_H , defined by $e_H[k] = \tilde{H}[k] - H[k - 1]$, $k \geq 0$. Substituting (12) into (14), we have

$$e_H[k + 1] = a[k]e_H[k] + b[k](H[k] - H[k - 1]), \quad (16)$$

where

$$a[k] \triangleq 1 - \frac{hc_1}{c_0(1 + g[k])}, \quad b[k] \triangleq \frac{\bar{g} - g[k]}{1 + g[k]}.$$

From (16), we compute

$$e_H[k + 1] = \left(\prod_{i=0}^k a[i]\right)e_H[0] + \sum_{i=0}^k \left(\prod_{j=i+1}^k a[j]\right)b[i](H[i] - H[i - 1]). \quad (17)$$

Since $e_H[0] = 0$,

$$\begin{aligned} |e_H[k+1]| &\leq 2\left(\sum_{i=0}^k \bar{a}^i\right)\bar{b} \|H\|_\infty \\ &\leq \frac{2\bar{b}}{1-\bar{a}} \|H\|_\infty, \end{aligned} \quad (18)$$

where

$$\bar{a} \triangleq \max_{x \in [0, C_g]} \left|1 - \frac{hc_1}{c_0(1+x)}\right|, \quad \bar{b} \triangleq \max_{x \in [0, C_g]} \left|\frac{\bar{g}-x}{1+x}\right|.$$

It's easy to verify that

$$\bar{a} = \max\left\{\frac{hc_1}{c_0} - 1, 1 - \frac{hc_1}{c_0(1+C_g)}\right\}, \quad \bar{b} = \max\left\{\bar{g}, \frac{C_g - \bar{g}}{1+C_g}\right\}.$$

Therefore $\|e_H\|_\infty \leq 2\bar{\gamma}_e \|H\|_\infty$. The error e_H can be thought of as the output of some uncertainty block Δ_H with the induced gain less than or equal to $2\bar{\gamma}_e$ (Figure 10(b)). But since Γ, Γ^{-1} sit outside the dashed box in Figure 10(b), we can not carry Δ_H along further. Instead we represent e_H as an exogenous disturbance with magnitude bounded by $2\bar{\gamma}_e r_0$ (Figure 10(c)). Eq. (15) now follows using the Lipschitz continuity and the time invariance properties of Γ . It's easy to see that the optimal \bar{g} minimizing the error bound is $\frac{C_g}{C_g+2}$. \square

Similarly we can derive the error bound for the implicit Euler algorithm (13):

Proposition 4.3 *Let the assumptions in Proposition 4.2 hold. Consider the implicit Euler algorithm (13). Then for any $M[\cdot] \in l_\infty$, for any $\psi_0 \in \Psi$,*

$$\|e_M\|_\infty \leq 2L_\mu \bar{\gamma}_i r_0, \quad (19)$$

where

$$\bar{\gamma}_i = \max\left\{\frac{\bar{g}}{1 + \frac{c_1 h}{c_0}}, \frac{C_g - \bar{g}}{1 + C_g + \frac{c_1 h}{c_0}}\right\} \frac{c_0(1+C_g) + c_1 h}{c_1 h}.$$

The optimal \bar{g} to minimize $\bar{\gamma}_i$ is $\frac{(c_0+c_1 h)C_g}{2(c_0+c_1 h)+c_0 C_g}$.

Remark 4.5 *For the explicit algorithm, the step size h has to be chosen small enough to ensure stability of (14) and (16). The implicit algorithm, however, is stable $\forall h > 0$. Therefore the implicit algorithm is preferred in general.*

Remark 4.6 *Propositions 4.2 and 4.3 use the Lipschitz continuity of the Preisach operator. We recall from [11] that if the Preisach measure is nonsingular, the Preisach operator will be continuous.*

Furthermore, if the measure ν satisfies the condition

$$\nu(N(\psi, \epsilon)) \leq \epsilon L_\mu, \quad \forall \psi \in \Psi, \quad (20)$$

for some $L_\mu > 0$, where $N(\psi, \epsilon)$ denotes the ϵ -neighbourhood of ψ , then the Preisach operator is Lipschitz continuous with the Lipschitz constant $2L_\mu$. The condition (20) is usually satisfied in practice.

Propositions 4.2 and 4.3 quantify the errors solely due to inversion algorithms. It's straightforward to extend the error estimates to the case that there are parametric uncertainties in c_0 and c_1 . The error due to inversion of the Preisach operator and to the uncertainty in the Preisach measure can also be included as done in Subsection 4.1.

When the square operator is present, like in the case of a magnetostrictive actuator, the estimate of e_u can be derived from that of e_M . Let $u \in [u_{min}, u_{max}]$ (recall Figure 1(b)), with $u_{min} \geq 0$. One can easily verify that

$$\|e_u\|_\infty \leq \|e_M\|_\infty^2 + 2\|e_M\|_\infty \sqrt{u_{max}}.$$

5 Formulation of the Robust Control Problem

In this paper, we consider $\hat{G}_0(\lambda)$ to be the identity operator, i.e., we are interested in trajectory tracking of the actuator head itself. Figure 11 shows the closed-loop system after the inverse compensation is done, where the exogenous noise v represents the inversion error. From the previous section, $\|v\|_\infty \leq \bar{v}$, and \bar{v} is quantifiable in terms of inverse schemes and parametric uncertainties. $\hat{G}_a(\lambda)$ stands for the discretized version of $G(s)$ in Figure 6. The composition $\Delta \circ \hat{W}_0(\lambda)$ represents the deviation of the actual plant from the nominal plant $\hat{G}_a(\lambda)$. We assume that Δ can be any nonlinear operator with $\|\Delta\|_{l_\infty-ind} < 1$, where $\|\cdot\|_{l_\infty-ind}$ denotes the induced operator norm when the signal space is l_∞ . $\hat{W}_0(\lambda)$ is a weighting function and it reflects that the model uncertainty is larger at a higher frequency.

Let $\|y_{ref}\|_\infty \leq \bar{r}$, where y_{ref} is the reference trajectory. The error $e_y \triangleq y_{ref} - y$ is fed into the controller $\hat{K}(\lambda)$. The delay λ following $\hat{K}(\lambda)$ is due to inversion of the dynamic hysteresis model. Let the saturation limits of the actuator be $-\bar{u}$ and \bar{u} respectively. Then the saturation constraint translates into $\|u_0\|_\infty \leq 1$, where u_0 is as defined in Figure 11. The case $u_{min} \neq -u_{max}$ will be discussed in Section 6.

1. the closed-loop system is stable for any Δ with $\|\Delta\|_{l_\infty-ind} < 1$,
2. $\|e_0\|_\infty \leq 1$ if $\Delta = 0$, $\forall v_0, r_0$ with $\|v_0\|_\infty \leq 1$ and $\|r_0\|_\infty \leq 1$, and
3. $\|u_0\|_\infty \leq 1$ if $\Delta = 0$, $\forall v_0, r_0$ with $\|v_0\|_\infty \leq 1$ and $\|r_0\|_\infty \leq 1$.

If we define the exogenous input w and the regulated output z as

$$w \triangleq \begin{pmatrix} v_0 \\ r_0 \end{pmatrix}, \quad z \triangleq \begin{pmatrix} e_0 \\ u_0 \end{pmatrix},$$

then items 2 and 3 above are equivalent to $\|\Phi_{zw}\|_1 \leq 1$, where Φ_{zw} denotes the transfer function from w to z , and $\|\cdot\|_1$ denotes the l_1 norm of a LTI system [2]. By the small gain theorem, (5) is equivalent to requiring robust stability of the system when we wrap a nonlinear uncertainty block Δ_P from z to w with $\|\Delta_P\|_{l_\infty-ind} < 1$, as shown in Figure 12 (b).

Now the control problem can be reformulated as: find the smallest γ and a stabilizing controller $\hat{K}(\lambda)$, such that the closed-loop system in Figure 12 (b) is robustly stable for all $\tilde{\Delta} \in \tilde{\mathbf{\Delta}}$, where $\tilde{\mathbf{\Delta}} \triangleq \{\tilde{\Delta} = \text{diag}(\Delta, \Delta_P) : \Delta \text{ is nonlinear and of dimension } 1 \times 1, \Delta_P \text{ is nonlinear and of dimension } 2 \times 2, \|\tilde{\Delta}\|_{l_\infty-ind} < 1\}$.

To solve the robust control problem, we need determine, for a fixed $\gamma > 0$, whether we can find a stabilizing $\hat{K}(\lambda)$, such that the closed-loop system is stable for all $\tilde{\Delta} \in \tilde{\mathbf{\Delta}}$. This will be called *the robust control problem with disturbance attenuation level γ* , and it is solvable if and only if

$$\inf_{\text{stabilizing } \hat{K}} \inf_{D \in \mathbf{D}} \|D^{-1}F_l(\hat{G}, \hat{K})D\|_1 \leq 1, \quad (23)$$

where $\mathbf{D} \triangleq \{D = \text{diag}(d_1, d_2, d_2) : d_1, d_2 > 0\}$, and $F_l(\cdot, \cdot)$ denotes the lower Linear Fractional Transformation [2]. We now give a sketch of how to solve (23). Interested readers are referred to [2] for details of the approach.

We restrict ourselves to finite dimensional LTI (FDLTI) controllers. Simultaneous optimization with respect to D and \hat{K} is hard, and a practical approach is to use the *D – K iteration* method and decompose the problem (23) into a sequence of decoupled optimization problems.

In Step 1 of each *D – K* iteration, for a fixed $D \in \mathbf{D}$, we want to solve

$$\inf_{\text{stabilizing } \hat{K}} \|D^{-1}F_l(\hat{G}, \hat{K})D\|_1. \quad (24)$$

Partition \hat{G} into a 2×2 block matrix as shown in (22) and denote it as

$$\hat{G} = \begin{pmatrix} \hat{G}_{11} & \hat{G}_{12} \\ \hat{G}_{21} & \hat{G}_{22} \end{pmatrix}.$$

Since \hat{G}_{22} for our problem is stable, the set of stabilizing FDLTI controllers \hat{K} is parametrized by:

$$\hat{K}(\lambda) = -\frac{Q}{1 - \hat{G}_{22}Q}, \quad Q \in \mathcal{RH}_{\infty}^{1 \times 1}, \quad (25)$$

and the scaled achievable closed-loop maps is parametrized by

$$D^{-1}F_l(\hat{G}, \hat{K})D = E - UQV, \quad Q \in \mathcal{RH}_{\infty}^{1 \times 1}, \quad (26)$$

where $E \triangleq D^{-1}\hat{G}_{11}D$, $U \triangleq D^{-1}\hat{G}_{12}$, $V \triangleq \hat{G}_{21}D$, and $\mathcal{RH}_{\infty}^{1 \times 1}$ denotes the space of real rational (complex) functions that are analytic on the open unit disc and bounded on the unit circle. Therefore (23) is transformed into

$$\inf_{Q \in \mathcal{RH}_{\infty}^{1 \times 1}} \|E - UQV\|_1. \quad (27)$$

Problem (27) is a multi-block l_1 model matching problem and we can approximate it by a one-block l_1 model matching problem through delay augmentation (DA). The latter problem is then solved using linear programming. We also obtain a sub-optimal controller for (26) from the DA method.

Remark 5.1 *For the system we consider, the only zeros that the delay augmented matrices U_N and V_N (c.f. [2]) have inside the unit disk are 0's. This has two pleasant consequences:*

1. *In computation of null chains and evaluation of the zero interpolation conditions, relevant coefficients can be obtained directly from the impulse responses and we thus avoid expensive symbolic calculation of high order derivatives.*
2. *From the zero interpolation conditions, the upper bound on the (finite) length of the closed-loop impulse response can be derived explicitly.*

In Step 2 of each $D - K$ iteration, an analytical expression for the optimal D^* exists since there are only two blocks in the structured uncertainty class $\tilde{\Delta}$.

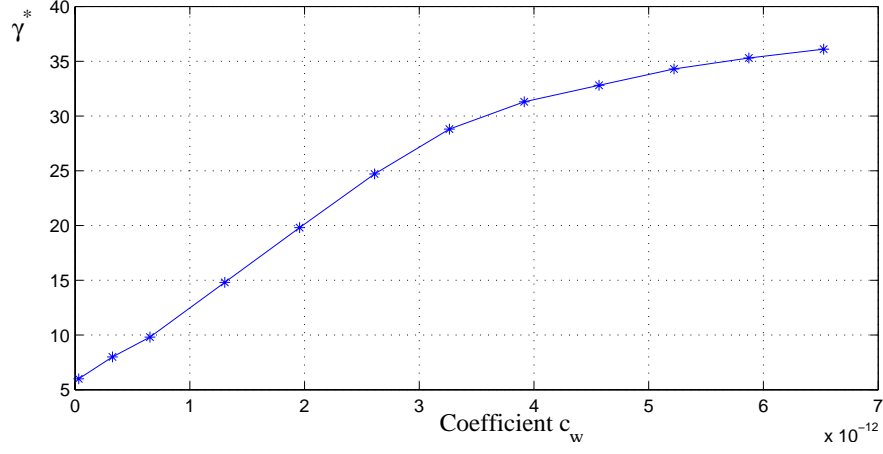


Figure 13: Effect of the model uncertainty on γ^* .

6 Simulation and Experimental Results

6.1 Effects of design parameters on the optimal disturbance attenuation level

We first present some computation results on how the optimal attenuation level γ^* is affected by the following factors: the magnitude of uncertainty, the magnitude \bar{v} of the inversion error, and the saturation limit \bar{u} .

The sampling frequency we use is 2000 Hz. The corresponding $\hat{G}_a(\lambda)$ is

$$\hat{G}_a(\lambda) = \frac{2.23 \times 10^{-11} \lambda^2 + 4.28 \times 10^{-11} \lambda}{0.147 \lambda^2 - 0.549 \lambda + 1}.$$

We choose the continuous time weighting function to be $W_0(s) = \frac{c_w(s+1)}{s+300}$, where $c_w > 0$ determines the magnitude of the uncertainty in the plant. Discretizing $W_0(s)$ gives

$$\hat{W}_0(\lambda) = \frac{1.1759 c_w (\lambda - 1.0005)}{\lambda - 1.1765}.$$

We let $\bar{r} = 30$.

Figure 13 shows the effect of the uncertainty magnitude on γ^* . Other parameters used are $\bar{v} = 0.1M_s^2$, $\bar{u} = 7.5M_s^2$, where M_s is the saturation magnetization. Since the range of u in the case of a magnetostrictive actuator is $[0, M_s^2]$ (recall Figure 6), expressing \bar{v} and \bar{u} in terms of M_s^2 allows one to make more concrete sense out of these numbers. From Figure 13, we see that the higher the uncertainty, the bigger γ^* .

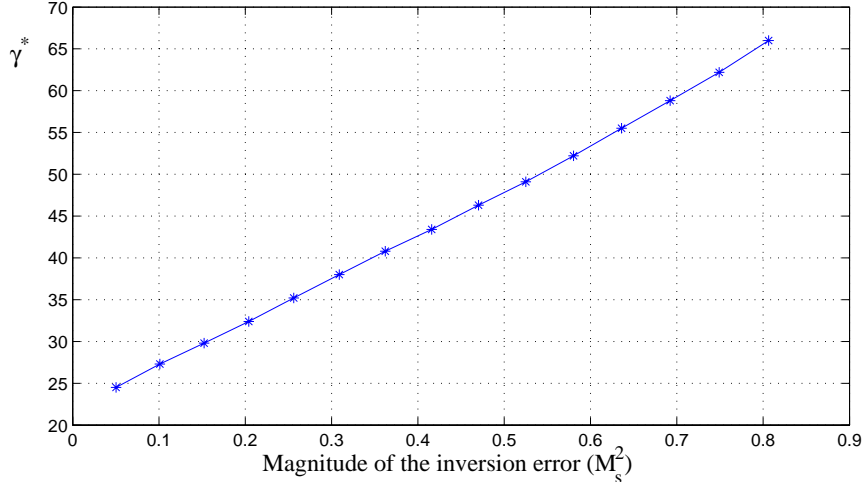


Figure 14: Effect of the inversion error on γ^* .

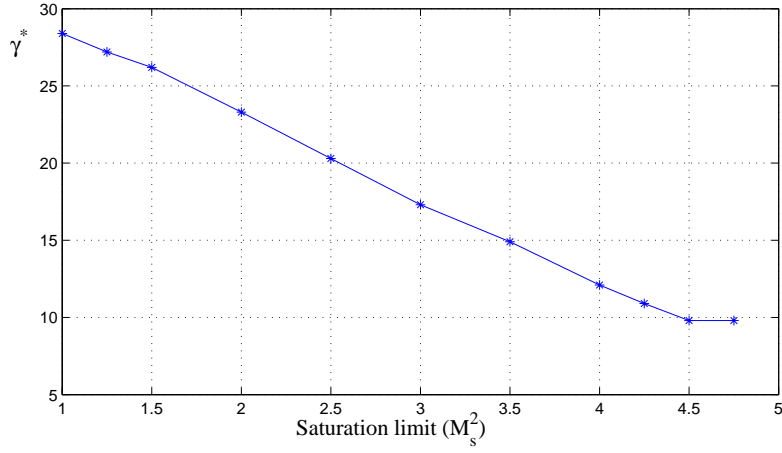


Figure 15: Effect of the saturation limit on γ^* .

Figure 14 displays how γ^* varies with the magnitude \bar{v} of the inversion error, where we have fixed $c_w = 6.53 \times 10^{-13}$ and $\bar{u} = 1.25M_s^2$. As one expects, the optimal attenuation level γ^* increases as \bar{v} increases.

Figure 15 shows how γ^* is affected by the saturation constraint. We have used $c_w = 6.53 \times 10^{-13}$ and $\bar{v} = 0.1M_s^2$. γ^* drops when \bar{u} increases, but γ^* becomes a constant when \bar{u} hits $4.5M_s^2$, beyond which the saturation constraint no longer plays a role.

6.2 Results of trajectory tracking

The saturation constraint considered so far is of the form $|u| \leq \bar{u}$. But for real actuators, the saturation limits may be asymmetric, i.e., $u_{min} \neq -u_{max}$. For example, for magnetostrictive actuators, $u \in [0, M_s^2]$. To handle the general constraint $u \in [u_{min}, u_{max}]$, we let $\bar{u} = \frac{u_{max} - u_{min}}{2}$ and $u_b = \frac{u_{max} + u_{min}}{2}$. The quantity \bar{u} is the saturation limit to be used in the controller design, while u_b is a bias input to be injected into the system. Then the actual control will be $u = u_c + u_b$ with $|u_c| \leq \bar{u}$.

Since the gain of \hat{W}_0 is close to 0 for a dc signal, we can ignore the contribution of u_b to the actuator output y through the $\Delta \circ \hat{W}_0$ branch. Its contribution through the \hat{G}_a branch can be calculated as

$$y_b = \frac{\lambda \hat{G}_a(\lambda)}{1 + \lambda \hat{K}(\lambda) \hat{G}_a(\lambda)} u_b.$$

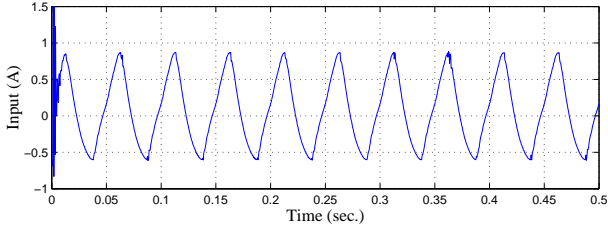
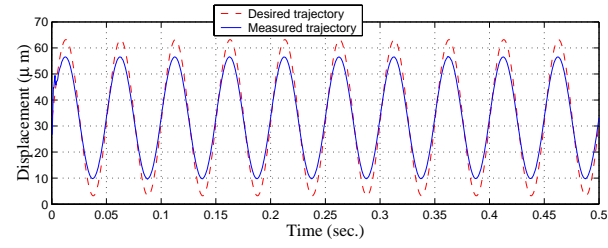
The previous robust control framework applies if we add y_b to the reference trajectory y_{ref} (or alternatively, taking y_b off from y).

As we have seen from Figure 15, the tracking performance deteriorates as the saturation constraint \bar{u} is tightened. For the magnetostrictive actuator, $\bar{u} = 0.5M_s^2$ and strictly enforcing this constraint will lead to large tracking errors. This reveals the limitation of pure linear design for an intrinsically nonlinear plant. Hence a practical approach would be to properly relax the constraint.

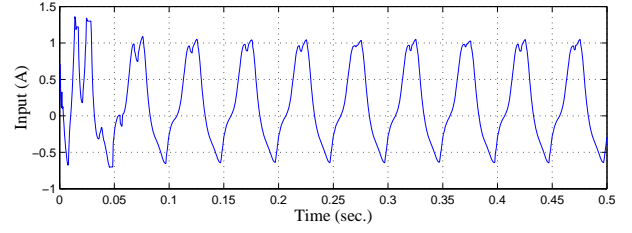
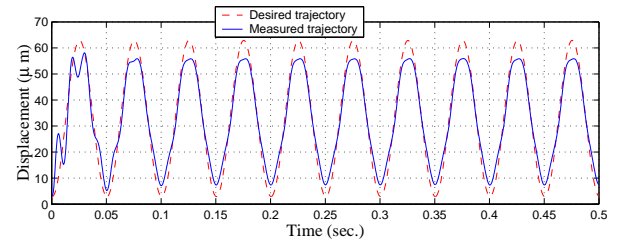
Figures 16(a) and 17(a) show the simulation results of tracking a sinusoidal signal and an irregular signal, respectively. The current I applied is also displayed. The controller $\hat{K}(\lambda)$ is designed based on $\bar{r} = 30$, $c_w = 3.3 \times 10^{-13}$, $\bar{v} = 0.1M_s^2$, and $\bar{u} = 3.25M_s^2$. Figure 18 shows the output of $\hat{K}(\lambda)$ in tracking the sinusoidal signal, and we see that although we set $\bar{u} = 3.25M_s^2$ in the controller design, the control stays in the (true) unsaturated region $[-0.5M_s^2, 0.5M_s^2]$ except during the transient period at the beginning.

Our composite controller (the linear robust controller plus the inverse algorithm) is computation efficient and we can implement it in real-time. Figures 16(b) and 17(b) show the experimental results of trajectory tracking based on the same controller used in the simulation. It matches well with the simulation result and the overall performance is satisfactory.

The saturation limit \bar{u} can not be “over-relaxed”. For example, we design another controller based on $\bar{r} = 25$, $c_w = 3.3 \times 10^{-13}$, $\bar{v} = 0.05M_s^2$, and $\bar{u} = 5M_s^2$. The simulation result (Figures 19(a)) based on this new controller is better than that in Figure 16(a). But when we put the controller into

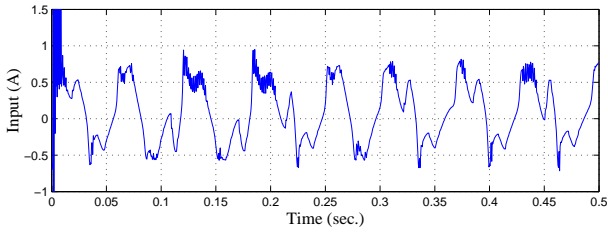
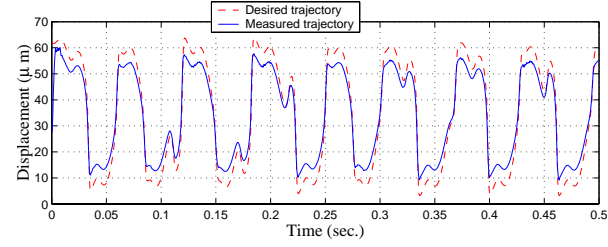


(a)

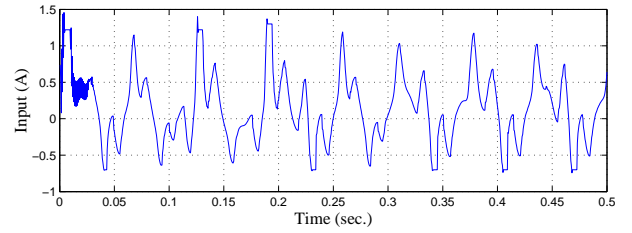
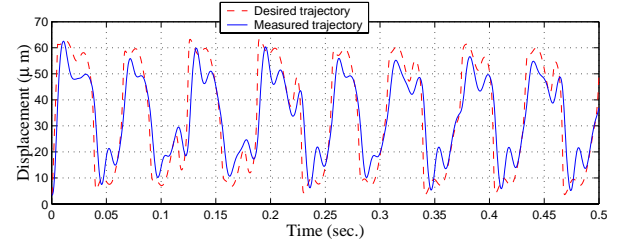


(b)

Figure 16: Results of tracking a sinusoidal signal. (a) Simulation result; (b) Experimental result.



(a)



(b)

Figure 17: Results of tracking an irregular signal. (a) Simulation result; (b) Experimental result.

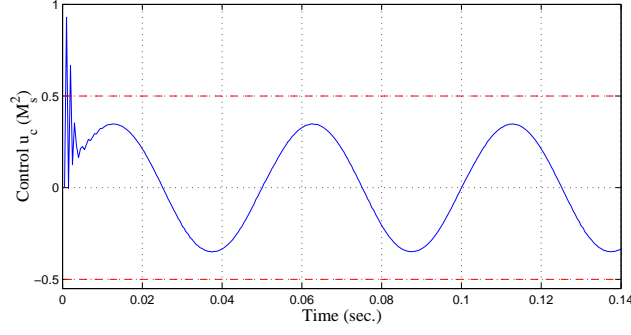


Figure 18: The control output u_0 in simulation of tracking the sinusoidal signal.

the experiment, the tracking performance suffers from the persistent saturation (Figure 19(b)). This justifies the necessity of including the saturation constraint in the problem formulation.

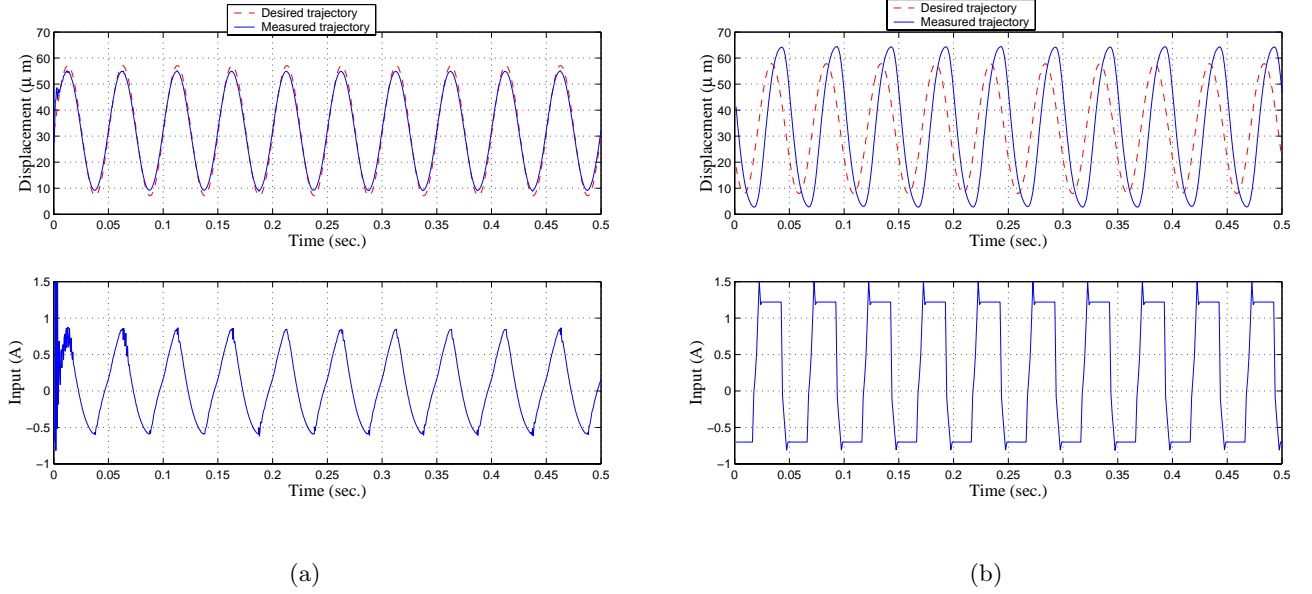


Figure 19: Results based on an “over-relaxed” controller. (a) Simulation result of trajectory tracking; (b) Experimental result of trajectory tracking.

7 Conclusions

In this paper, we presented a robust control framework for smart actuators by combining the inverse compensation with the linear robust control theory, where the essential ideas were illustrated through the example of robust tracking of a magnetostrictive actuator.

We first showed that, the inversion error for a Preisach operator-based hysteresis model, either rate-independent or rate-dependent, can be bounded in magnitude. Furthermore, the bound can be characterized in terms of parameter uncertainties and the specific inversion scheme used. This allows us to model the inversion error as an exogenous noise and attenuate its impact by robust control techniques.

We then aimed to achieve three competing goals in the robust control problem formulation: robust stability, robust tracking, and not exceeding the saturation constraint. We also discussed how to balance these goals and seek the sensible trade-off. Simulation and experimental results have demonstrated the effectiveness of the robust control scheme.

Acknowledgements

This research was supported by the Army Research Office under the ODDR&E MURI97 Program Grant No. DAAG55-97-1-0114 to the Center for Dynamics and Control of Smart Structures (through Harvard University). The authors would like to acknowledge useful discussions with Prof. R. Venkataraman, Prof. P. S. Krishnaprasad and Prof. A. Tits.

References

- [1] R. Venkataraman and P. S. Krishnaprasad, “Approximate inversion of hysteresis: theory and numerical results,” in *Proceedings of the 39th IEEE Conference on Decision and Control*, Sydney, Australia, Dec. 2000, pp. 4448–4454.
- [2] M. A. Dahleh and I. J. Diaz-Bobillo, *Control of Uncertain Systems: A Linear Programming Approach*, Prentice-Hall, Englewood Cliffs, NJ, 1995.
- [3] D. Hughes and J. T. Wen, “Preisach modeling and compensation for smart material hysteresis,” in *Active Materials and Smart Structures*, G. L. Anderson and D. C. Lagoudas, Eds., 1994, vol. 2427 of *SPIE*, pp. 50–64.
- [4] G. Tao and P. V. Kokotović, “Adaptive control of plants with unknown hysteresis,” *IEEE Transactions on Automatic Control*, vol. 40, no. 2, pp. 200–212, 1995.

- [5] R. C. Smith, “Inverse compensation for hysteresis in magnetostrictive transducers,” Tech. Rep. CRSC-TR98-36, CRSC, North Carolina State University, 1998.
- [6] W. S. Galinaitis and R. C. Rogers, “Control of a hysteretic actuator using inverse hysteresis compensation,” in *Mathematics and Control in Smart Structures*, V.V. Varadan, Ed., 1998, vol. 3323 of *SPIE*, pp. 267–277.
- [7] X. Tan, R. Venkataraman, and P. S. Krishnaprasad, “Control of hysteresis: Theory and experimental results,” in *Modeling, Signal Processing, and Control in Smart Structures*, V. S. Rao, Ed., 2001, vol. 4326 of *SPIE*, pp. 101–112.
- [8] P. Ge and M. Jouaneh, “Tracking control of a piezoceramic actuator,” *IEEE Transactions on Control Systems Technology*, vol. 4, no. 3, pp. 209–216, 1996.
- [9] R. B. Gorbet, D. W. L. Wang, and K. A. Morris, “Preisach model identification of a two-wire SMA actuator,” in *Proceedings of IEEE International Conference on Robotics and Automation*, 1998, pp. 2161–2167.
- [10] I. D. Mayergoyz, *Mathematical Models of Hysteresis*, Springer Verlag, 1991.
- [11] A. Visintin, *Differential Models of Hysteresis*, Springer, 1994.
- [12] M. Brokate and J. Sprekels, *Hysteresis and Phase Transitions*, Springer Verlag, New York, 1996.
- [13] X. Tan and J. S. Baras, “Control of hysteresis in smart actuators, Part I: Modeling, parameter identification, and inverse control,” submitted to *Automatica*, 2002.
- [14] G. Tao and P. V. Kokotović, *Adaptive Control of Systems with Actuator and Sensor Nonlinearities*, John Wiley & Sons, Inc, 1996.
- [15] K. Kuhnen and H. Janocha, “Adaptive inverse control of piezoelectric actuators with hysteresis operators,” in *Proceedings of European Control Conference (ECC)*, Karlsruhe, Germany, 1999, Paper F 0291.
- [16] X. Tan and J. S. Baras, “A robust control framework for smart actuators,” submitted to 2003 American Control Conference.
- [17] H. L. Royden, *Real Analysis*, Prentice Hall, Englewood Cliffs, NJ, 1988.

- [18] X. Tan, *Control of Smart Actuators*, Ph.D. thesis, University of Maryland, College Park, MD, Sept. 2002, available online at http://techreports.isr.umd.edu/TechReports/ISR/2002/PhD_2002-8/PhD_2002-8.phtml.
- [19] R. Venkataraman, *Modeling and Adaptive Control of Magnetostrictive Actuators*, Ph.D. thesis, University of Maryland, College Park, 1999.
- [20] R. Venkataraman and P. S. Krishnaprasad, “A model for a thin magnetostrictive actuator,” in *Proceedings of the 32nd Conference on Information Sciences and Systems, Princeton, NJ*, Princeton, Mar. 1998.